This document is the Accepted Manuscript version of a Published Work that appeared in final form in Analytical Chemistry. To access the final edited and published work see https://doi.org/10.1021/acs.analchem.2c02523.

Investigating comproportionation in multi-electron transfers via UV-vis spectroelectrochemistry: The electro-reduction of anthraquinone-2-sulfonate in aqueous media

Luis Romay, Joaquín González, Ángela Molina, Eduardo Laborda*

Departamento de Química Física, Facultad de Química, Regional Campus of International Excellence "Campus Mare Nostrum", Universidad de Murcia, 30100 Murcia, Spain

* Corresponding author: elaborda@um.es

ABSTRACT

UV-vis spectroelectrochemistry is assessed as a tool for the diagnosis and quantitative *in situ* investigation of the incidence of comproportionation in multi-electron transfer processes. Thus, the sensitivity of the limiting current chronoabsorptometric signals related to the different redox states to the comproportionation kinetics is studied theoretically for different working modes (normal and parallel light beam arrangements) and mass transport regimes (from semi-infinite to thin layer diffusion).

The theoretical results are applied to the spectroelectrochemical study of the two-electron reduction of the anthraquinone-2-sulfonate in alkaline aqueous solution, tuning the thermodynamic favourability of the comproportionation reaction through the electrolyte cation. The quantitative analysis of the experimental results reveals the occurrence of comproportionation in the three media examined, showing different kinetics depending on the cationic species in solution.

Anthraquinones (AQs) and other quinone derivatives are of great interest given their role in a myriad of applications: production of hydrogen peroxide[1,2], energy storage devices[3–6], anticancer, antibacterial or antimalarial agents[7–10], photocatalysis[11], wastewater treatment[12], pest management[13],… In these contexts, understanding and even controlling the electrochemical behaviour of AQs is crucial. For example, the toxicity of AQs has been ascribed, among other factors, to the formation of the singly-reduced form (semiquinone radical) that reduces oxygen to superoxide radicals[14]. The predominant product of the AQ (electro)reduction is determined by the AQ chemical structure and also by the medium that stabilizes distinctly the different redox forms via hydrogen bonding, protonation, ion pairing, complexation,…[15,16]. Assuming that such processes are fast enough, equilibrium conditions can be presumed and the electro-reduction mechanism addressed as an 'apparent' EE mechanism with conditional values of the formal potentials dependent on the solution composition[17]:

$$\begin{aligned} AQ + e^- &\rightleftharpoons AQ^{\bullet -} \ , \ E^{0'}_{1,app} \\ AQ^{\bullet -} + e^- &\rightleftharpoons AQ^{2-} \ , \ E^{0'}_{2,app} \end{aligned} \qquad (1)$$

An additional relevant aspect to be considered (as in any electrochemical system involving multiple electron transfers and redox couples[18–20]) is the impact of comproportionation-disproportionation (COMP-DISP) reactions in solution[21–24]:

$$AQ + AQ^{2-} \underset{k_{disp}}{\overset{k_{comp}}{\rightleftharpoons}} 2AQ^{\bullet -} \qquad (2)$$

The extent of COMP-DISP will be defined by the difference between the apparent formal potentials: $K = \exp\left(-\frac{F\Delta E^{0'}_{app}}{RT}\right)$ with $\Delta E^{0'}_{app} = E^{0'}_{2,app} - E^{0'}_{1,app}$. Thus, COMP will dominate when the formal potentials follow the "normal ordering" (*i.e.*, $E^{0'}_{2,app} < E^{0'}_{1,app}$, $\Delta E^{0'}_{app} < 0$), while DISP will prevail in the situation of so-called "inverted ordering" ($E^{0'}_{2,app} > E^{0'}_{1,app}$, $\Delta E^{0'}_{app} > 0$) [25].

Voltammetric techniques are generally very powerful in the investigation of the redox mechanisms and activity of chemical compounds. Nevertheless, there are some aspects where they are unable to provide accurate information, or even information at all. Within the present context, it is well known that the voltammetry of diffusion-only multi-electron transfers is no[26] or scarcely[27,28] sensitive to COMP-DISP processes since the "average oxidation state" in solution is not altered[22]. In order to overcome this limitation, voltammetry in weakly supported media has been applied[29], on the basis of the different mass transport by migration of the different redox forms in (1)-(2) as long as they are differently charged. Alternatively, in this work the use of UV-vis spectroelectrochemistry (SEC) is investigated. SEC can provide *in situ* and real-time

direct evidence of the formation or consumption of chemical species and so assist the unambiguous elucidation of intricate electrochemical mechanisms[30–32]. Within the present context, as the concentration profiles of the redox forms are affected by the DISP-COMP reactions (see below and [29,33]), the species-sensitive absorbance signal can enable us to reveal and characterize COMP-DISP processes under diffusion-only conditions and with direct access to the species concentrations, which can make the modelling, interpretation of results and data analysis more simple, conclusive and accurate. This is examined theoretically in the first part of the manuscript for a generic two-electron transfer under different mass transport conditions and SEC arrangements; thus, the parallel and normal light beam modes are examined (see Figure S1), where the former is generally more advantageous since it enables the use of opaque electrodes, as well as higher absorbance signals. With regard to the electrochemical method, the simplest potential-controlled perturbation is considered: limiting current chronoamperometry. As discussed below, this allows for the reduction of the number of unknown parameters and of experimental uncertainty with respect to voltammetric techniques. In the second part, the electro-reduction of anthraquinone-2-sulfonate in alkaline aqueous media is studied experimentally in the presence of different electrolyte cations, which enables us to tune readily the $\Delta E_{app}^{0'}$ -value [16]. In all cases, the analysis and fitting of the experimental UV-vis absorbance signal clearly indicate the formation of the semiquinone intermediate via rapid comproportionation in solution. The results set the ground for the SEC study of transient and product species in multi-electron transfers, which can offer high capabilities given the wide variety of techniques available (EPR/ESR, Raman scattering, NMR, luminescence,…)[34–36] as well as the real-time, local, *in situ/operando* information of the system.

EXPERIMENTAL SECTION

Spectroelectrochemical experimental measurements were carried out with a SPELEC UV-vis instrument (200-900 nm, Metrohm-DropSens) in parallel mode under thin-layer diffusion conditions (see Scheme 1). For this, two bare optical fibers (100 µm core size, numerical aperture=0.22, Ocean Optics) were aligned and glued on the surface of the 4 mm-diameter gold working electrode of a screen-printed electrode 220BT (Metrohm-DropSens), which includes a gold auxiliary electrode and a silver pseudo-reference electrode (Figure S3). The alignment of the fibers was carried out by hand, searching for the maximum number of counts registered with the SPELEC instrument; subsequently, the alignment was confirmed from optical microscope images (Figure S3). Then, one of the fibers was connected to the light source of the SPELEC instrument and the other fiber to its spectrometer. The distance between the ends of the two optical fibers, which defines the length of the optical path (ℓ), was determined from images obtained with a Leica Z6 Apo macroscope and analyzed with ImageJ software: $\ell = 0.63$ mm (see Figure S3).

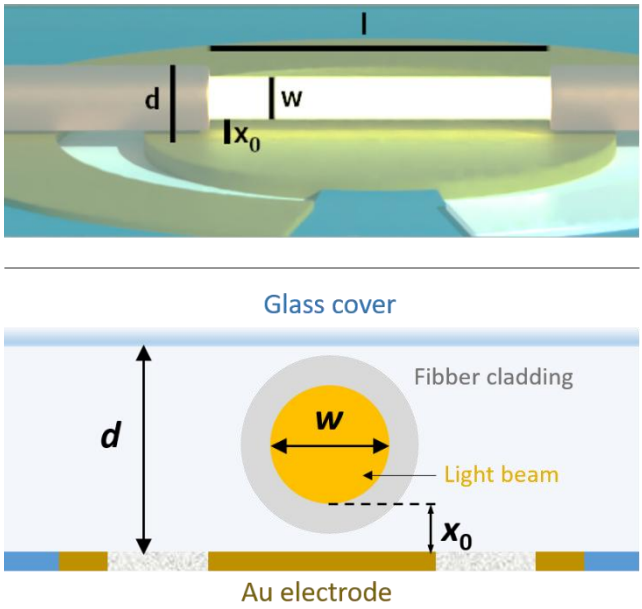

Scheme 1. Schematic of the working cell employed for the SEC experiments.

The fiber-modified screen-printed device was placed in a TRANSCELL (Metrohm-DropSens), 40 µL solution was dropped covering the surface of the three electrodes and, subsequently, a glass plate was placed on top and fixed by the top cover of the cell so ensuring a well-defined, uniform and reproducible thin-layer domain (see Figure S4). The distance between the thickness of the diffusion domain (d) and the distance between the electrode surface and the light beam (x_0) were determined from the fitting of simulated and experimental the diffusion-controlled chronoamperometric SEC signal at 420 nm [37] accompanying the electro-

oxidation of 3.7 mM ferrocyanide in a 1 M KNO_3 aqueous solution, as a model system (see Figure S5, and Section S4 for the details of the numerical simulation). The values obtained were $d = 175\ \mu m$ and $x_0 = 50\ \mu m$.

All SEC measurements were performed at room temperature, and the spectra registered were filtered using the standard Savitzky–Golay filter of the instrument (10 points and 1 degree polynomial), which was confirmed not to distort the features of the raw signal. In the case of the AQ solutions, atmospheric oxygen was removed by thorough bubbling of argon (Premier, Carburos Metálicos, 99,9992%) and subsequent potentiostatic electrolysis of O_2 traces prior to measurements, maintaining an Ar flux over the electrode system throughout the experiments (see Figure S4).

RESULTS AND DISCUSSION

Simulated UV-vis SEC spectroelectrochemistry

The SEC of a generic two-electron transfer

$$\begin{aligned} &A + e^- \rightleftarrows B \quad , E^{0'}_{1,app} \\ &B + e^- \rightleftarrows C \quad , E^{0'}_{2,app} \\ &A+C \underset{k_{disp}}{\overset{k_{comp}}{\rightleftarrows}} 2B \ , K = \exp\left(-\frac{F\Delta E^{0'}_{app}}{RT}\right) \text{ with } \Delta E^{0'}_{app} = E^{0'}_{2,app} - E^{0'}_{1,app} \end{aligned} \quad (3)$$

under diffusive mass transport is investigated theoretically (simulation details discussed in Section S3). A variety of situations can be envisaged, primarily depending on whether COMP or DISP is thermodynamically favourable, and on the relative absorptivity of the different electroactive species and the thickness of the diffusion domain. Among the multiple techniques available, limiting current chronoamperometry (CA) will be here considered where the applied potential, *E*, is notably more negative than $E^{0'}_{1,app}$ and $E^{0'}_{2,app}$ so that species A is electro-reduced to C, its interfacial concentration is null and species B is not generated at the electrode. The corresponding SEC-CA response is independent of the specific kinetics of the two electron transfers and of the specific value of the applied potential (provided that *E* is negative enough). This is very advantageous in the present context since it enables us to reduce the number of unknown parameters, and the system's response is independent of the exact applied potential (as long as it is negative enough) providing high tolerance to uncertainties associated to the use of pseudo-reference electrodes. A typical width of the light beam of w = 100 μm is considered.

Let us consider first the situation where comproportionation is thermodynamically favourable, for example, $\Delta E^{0'}_{app} = -200$ mV. The change in the parallel-mode absorbance with respect to its initial value ($\Delta A_p = A_p(t) - A_p(t=0)$ with $A_p(t=0) = \varepsilon_A \ell c^*_A$) is shown in Figure 1 at wavelengths where the predominant photoactive species is A (Figs. 1A and 1D), B (Figs. 1B and 1E) or C (Figs. 1C and 1F) under thin-layer ($d = 150$ μm, Figs. 1A-1C) or semi-infinite (Figs. 1D-1F) diffusion conditions; other situations in terms of absorptivity of the different redox species are given in Figure S7. The concentration profiles of the three species are shown in Figure 2 in the absence (Figs 2A-2C) and presence (Figs 2D-2F) of COMP, where small values of $T = t\,D_A / d^2$ correspond to semi-infinite diffusion and thin-layer effects are more apparent as T is larger.

Regardless of the diffusion regime and of the COMP kinetics (k_{comp}), when the main absorbing species is the reactant (A) or product (C) of the electrode reaction, ΔA_p decreases or increases with time, respectively, in a monotonous way towards the value corresponding to the

bulk electrolysis of A to C, $\Delta A_p = (\varepsilon_C - \varepsilon_A)\ell c_A^*$ (see Fig. 2). Such value is attained in tens of seconds under thin-layer conditions (Figs. 1A and 1C) while, in general, it requires atypically long times in the case of semi-infinite diffusion (Figs. 1D and 1F). Regarding the influence of the COMP kinetics, as k_{comp} is faster, species A and C are consumed more rapidly in the solution-phase COMP reaction (compare Figs. 2A *vs* 2D and 2C *vs* 2F). As a result, for a given intermediate time value, ΔA_p decreases as k_{comp} is larger (Figs. 1A, 1C, 1D and 1F) up to the limit of very fast COMP kinetics (k_{comp}>10^6 $M^{-1}s^{-1}$ in Figs. 1 and 2) where the occurrence of the COMP reaction is limited by the availability of species A (Fig. 2D).

At a wavelength where the absorbance is primarily associated to the intermediate species B (Figs. 1B and 1E), the ΔA_p-time response can show a more complex behaviour. Thus, in the absence of COMP (black line in Figs. 1B and 1E), species B is not generated at the applied potential considered either electrochemically or chemically (see Fig. 2B) and any change in ΔA_p is only due to the decrease of the concentration of A and the increase of the concentration of C; therefore, in Figs. 1B and 1E, where it is considered that $\varepsilon_C > \varepsilon_A$, there is a continuous increase of ΔA_p.

When COMP takes place, species B is produced chemically in solution and, simultaneously, it is fully reduced at the electrode surface ($E << E^{0'}_{2,app}$). As a result of the interplay between these two opposing processes, the amount of species B in solution initially increases when 'soft' thin-layer or semi-infinite conditions hold (Figs. 2B and 2E for T< 0.1); this gives rise to the corresponding increase of ΔA_p (Figs. 1B and 1E) since the medium is more absorbing ($\varepsilon_B > \varepsilon_C > \varepsilon_A$). As thin layer effects are more significant (larger *T* in Figs. 2B and 2E) and/or the COMP kinetics is faster (larger k_{comp} in Figs. 1B and 1E), the depletion of species A limits the COMP reaction so that the electrolysis of B dominates and its concentration decreases with time. Consequently, the ΔA_p-value shows a maximum that is more apparent and appears earlier as the COMP reaction is faster up to reaching the limit of very fast kinetics (k_{comp} >10^6 $M^{-1}s^{-1}$ under the conditions of Figure 1). As shown in Figure S8B, the characteristic maximum that reveals the incidence of COMP is enhanced under strong thin layer conditions where concentration changes are more notable since the diffusion of species B away from the electrode is constrained. For the same reason, in all cases (Fig. S8A-S8C) the ΔA_p-value reaches the bulk electrolysis limit ($\Delta A_p = (\varepsilon_C - \varepsilon_A)\ell c_A^*$) earlier as the thickness of the diffusion layer is decreased.

In Figure S9, the influence of $\Delta E_{app}^{0'}$ on the thin-layer ΔA_p-time responses in the presence of COMP-DISP is shown; the responses in the absence of COMP-DISP (grey dashed line) are also plotted for comparison. As the $\Delta E_{app}^{0'}$-value is more positive, the COMP reaction is thermodynamically less favourable (Eq. (3)) so that the effects discussed above are less significant, eventually vanishing for very positive $\Delta E_{app}^{0'}$ (black line). Note that the DISP reaction does not affect the signal in limiting current CA given that, at the applied potential considered, the formation of species B is not thermodynamically favourable, either electrochemically or chemically.

As shown in Figure S10, the influence of the COMP reaction on the chronoamperometric SEC signal is qualitatively the same in the parallel and normal modes, including the appearance of the maximum when the intermediate is the most absorbing form. Hence, the main difference between the two working modes is the smaller magnitude of the ΔA_p-values in the normal-beam arrangement for the generally smaller optical path length. This can lead to problems of optical sensitivity that could be addressed with larger diffusion domains and longer electrolysis (see Figure S11).

According to all the above, it can be concluded that the ΔA_p-times response at a wavelength (primarily) associated to species B is the most appropriate for the analysis of COMP since it shows a distinctive maximum, especially under thin-layer conditions, highly sensitive to k_{comp}. The ΔA_p–time response related to the consumption of A also shows notable sensitivity to COMP in any diffusion regime and in both parallel- and normal-beam arrangements. On the other hand, the ΔA_p signal related to the generation of the product C is the least informative and sensitive.

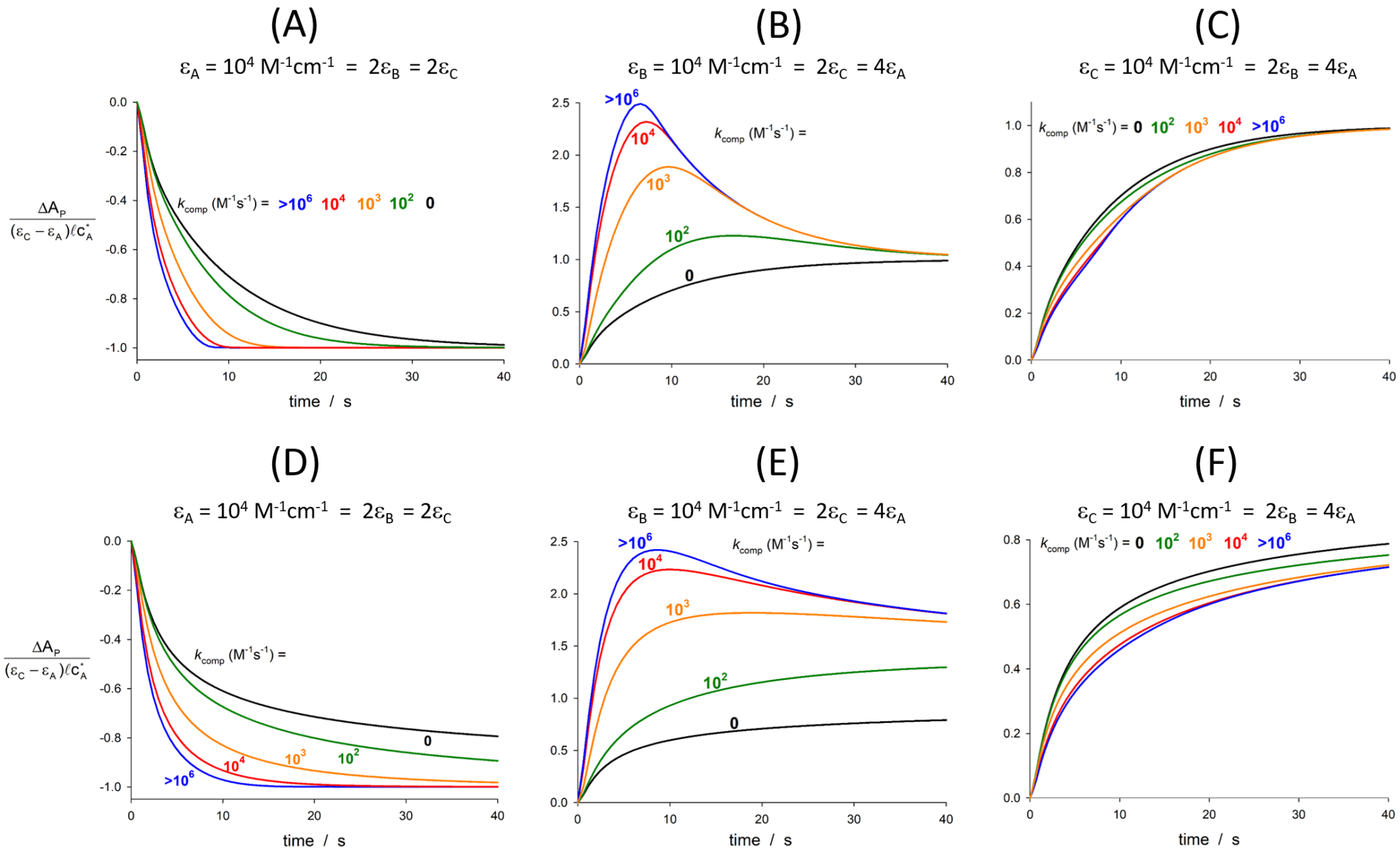

Figure 1. Absorbance-time signals as a function of the COMP kinetics in parallel SEC mode under **(A-C)** thin-layer ($d = 150$ μm) or **(D-F)** semi-infinite diffusion. $\ell = 0.1$ cm, $x_0 = 25$ μm, $\Delta E^{0'}_{app} = -200$ mV, $c^*_A = 1$ mM, $D_A = D_B = D_C = 10^{-5}$ cm^2 / s, T = 298 K. ε -values indicated on each graph.

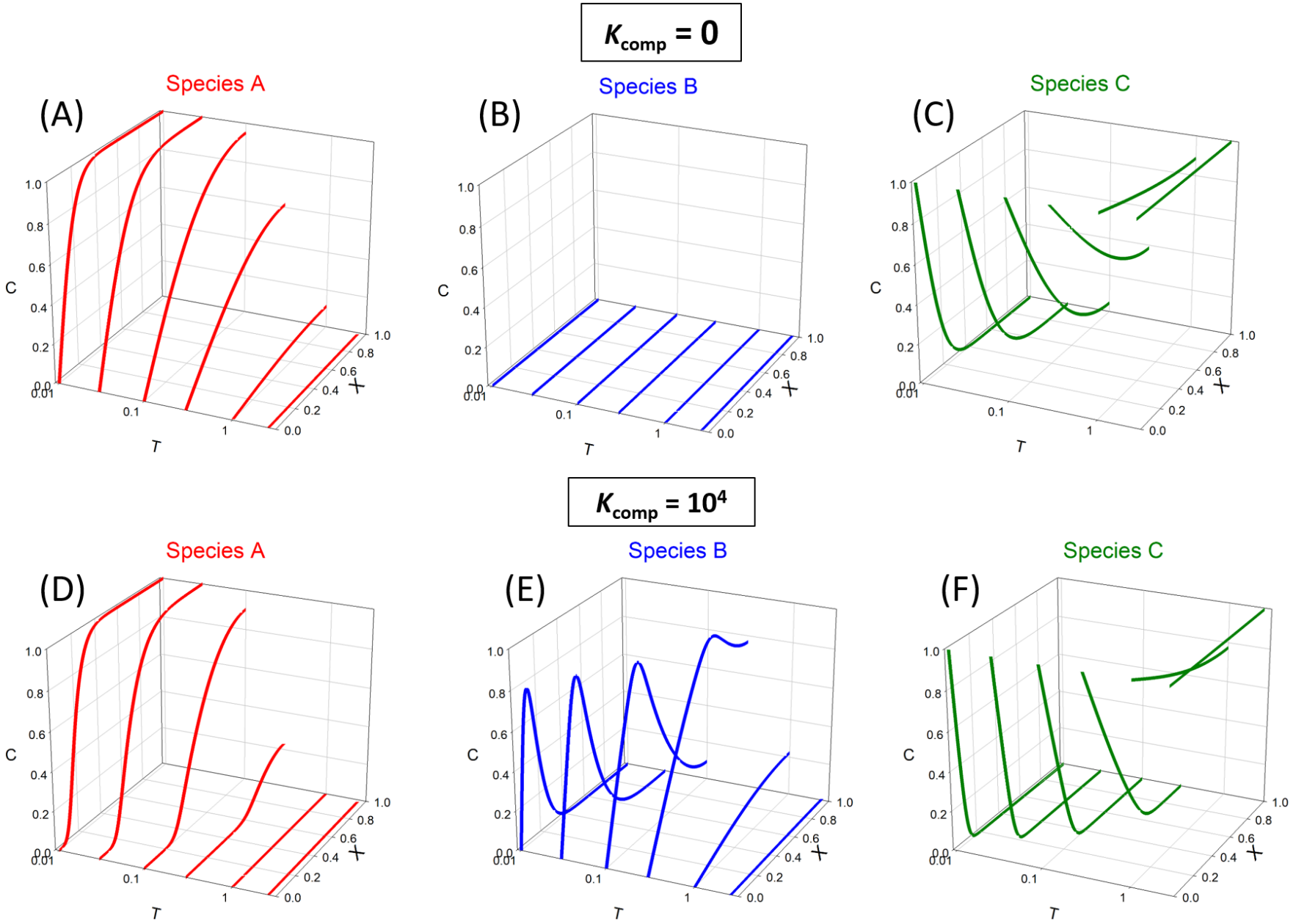

Figure 2. Dimensionless concentration profiles of the EE mechanism in limiting current CA with **(A-C)** no COMP or **(D-F)** very fast COMP. $D_A = D_B = D_C = 10^{-5}$ cm^2 / s, T = 298 K. See Table S1 for the definitions of the dimensionless magnitudes *C*, *X* and *T*.

3.2. Experimental study

Chronoabsorptometric experiments were conducted under limiting current conditions ($E = -0.85$ V (*vs* SCE), see Figure S2) for the electroreduction of anthraquinone-2-sulfonate in three different media: KOH, TMAOH or TBAOH aqueous alkaline solutions (pH > 13). Under such conditions, the different redox forms are deprotonated (pK_a's ≤ 11 [38]) and their ion pairing with the distinct electrolyte cation (K^+, TMA^+ or TBA^+) leads to different values of $\Delta E_{app}^{0'}$: -177 mV in TBAOH, -35 mV in TMAOH and -25 mV in KOH. Hence, the comproportionation reaction (2) is thermodynamically more favourable in the TBAOH solution.

With regard to the SEC arrangement, the parallel mode was preferred given that it usually offers higher optical sensitivity than the normal mode (see Figures S9A-C *vs* S9D-F) for the longer optical path length and, also, it enables the use of 'opaque' electrodes that offered better electrochemical responses.

Figure 3A shows the evolution of a representative spectra with time, where the spectrum of the initial solution has been taken as a reference (*i.e.*, $\Delta A_p = A_p(t) - A_p(t=0)$). At $\lambda = 330$ nm, ΔA_p decreases monotonously with time and reaches a constant negative value after *ca*. 30 s (see also Fig. S5B). As discussed above, this behaviour points out that the reactant $AQ2S^-$ is the main absorbing species at 330 nm, in agreement with its UV-vis spectrum (Figure S12 and [38]). Additionally, two maxima can be identified at $\lambda \simeq$ 430 and 500 nm. At 430 nm, ΔA_p increases continuously with time as corresponds to a wavelength where the absorbance of the fully reduced species $AQ2S^{3-}$ is higher than that of the reactant and intermediate. On the other hand, at 500 nm the ΔA_p-time plot shows a maximum (see also Fig. S5D) that is consistent with the incidence of the COMP reaction (2) with the intermediate $AQ2S^{\bullet 2-}$ being the most absorbing species. The latter is also in agreement with the literature where it is found that the intermediate species absorbs approximately twice as much as the fully reduced form at 500 nm [38].

The quantitative analysis of the COMP reaction in the electro-reduction of $AQ2S^-$ was performed by fitting the simulated and experimental ΔA_p *vs* time responses at 500 nm with ε_B, ε_C and k_{comp} as adjustable parameters; the two former mainly affect the magnitude of ΔA_p, while the latter determines the ΔA_p-time pattern. As can be seen in Figures 3B-3D, in the three media investigated, the experimental ΔA_p-time plot (blue circles) shows a maximum at *ca*. 20-30 s, which is more notorious as COMP is thermodynamically more favourable, that is, TBAOH > TMAOH > KOH. In all cases, a satisfactory agreement is reached between the experimental and simulated (red line) curves with the values indicated in Table 1. The values

obtained for k_{comp} point out that the comproportionation of $AQ2S^{-}$ and $AQ2S^{3-}$ is significant and fast in all the aqueous media investigated, as also reported in acetonitrile [29]. Moreover, the COMP kinetics is found to be dependent on the cationic species in solution, following the same order as that found for the ion pairing with the electrolyte cation [16], which would enhance the second-order kinetics between like-charged species ($AQ2S^{-}$ and $AQ2S^{3-}$) somehow in analogy to a kinetic salt effect.

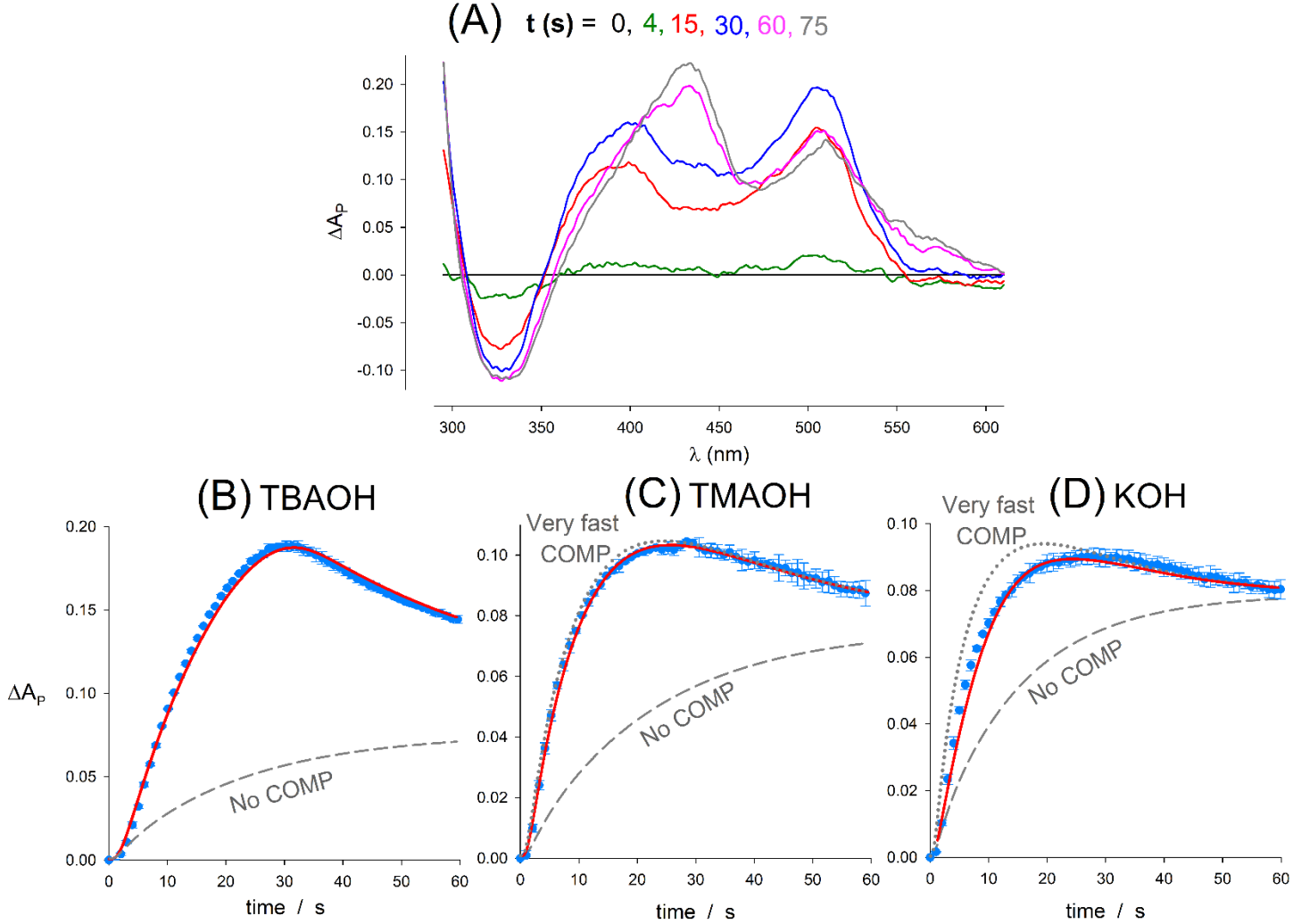

Figure 3. (A) Experimental ΔA_p *vs* λ spectra during a thin-layer CA-SEC experiment with a 0.35 mM $AQ2S^-$ 0.2 M TBAOH solution. **(B-D)** Experimental (blue circles) and best-fit simulated (red line) ΔA_p *vs* time responses at λ = 500 nm corresponding to 0.35 mM $AQ2S^-$ solutions with different electrolytes (indicated on each graph). The theoretical response predicted in the absence of COMP (*i.e.*, k_{comp} = 0 $M^{-1}s^{-1}$, grey dashed line) and for very fast COMP (grey dotted line) are also plotted for comparison; the latter overlaps with the red line in Fig. 3B. The error bars correspond to the standard deviation of three independent experiments.

Table 1. Parameters corresponding to the best-fit simulations in Figure 3.

$\varepsilon_C/10^3$ ($M^{-1}cm^{-1}$)	$\varepsilon_B / \varepsilon_C$	k_{comp} ($M^{-1}s^{-1}$)	*Root mean square error*
TBAOH			
4.4	2.15	$> 10^5$	$3.6x10^{-3}$
TMAOH			
3.5	2.05	$3 x 10^3$	$1.1x10^{-3}$
KOH			
3.5	1.8	600	$2.4x10^{-3}$

- The values of x_0, ℓ , d and D values were determined as detailed in the Experimental Section and in Section S1; the diffusion coefficients of the reduced species were assumed to be equal to that obtained for the reactant $AQ2S^-$.
- $\Delta E_{app}^{0'}$ as determined from the cyclic voltammetry under conventional semi-infinite diffusion conditions: -177 mV in TBAOH, -35 mV in TMAOH and -25 mV in KOH (Section S1.2).
- $\varepsilon_A = 0$ $M^{-1}s^{-1}$ according to the UV-vis spectrum of $AQ2S^-$ in aqueous alkaline solution (Figure S12 and [38]).

CONCLUSIONS

UV-vis spectroelectrochemistry allows for the detection and characterization of comproportionation (COMP) in multi-electron transfers. Taking into account the interplay of diffusive mass transport, chemical and electrochemical phenomena, the patterns of the parallel-mode UV-vis spectroelectrochemical signal in the simplest potential-controlled technique of limiting current chronoamperometry (CA) have been theoretically described. The absorbance-time response at wavelengths where the intermediate is the main absorbing species is found to be particularly convenient since it shows a characteristic non-monotonous behaviour when comproportionation takes place, allowing for the quantitative study of the COMP kinetics.

The parallel-mode, thin-layer CA spectroelectrochemical method has been applied successfully to the experimental study of the two-electron reduction of anthraquinone-2-sulfonate in different alkaline aqueous media, tuning the extent of the COMP reaction through the ion pairing with the base cation. In all the cases investigated, the fitting of the theoretical and experimental SEC signals reveals the formation of the semiquinone intermediate in solution by the (very) fast COMP of the anthraquinone with its doubly-reduced form. Such reaction is found to be favoured, both thermodynamically and kinetically, by ion pairing media.

SUPPORTING INFORMATION

Experimental details, simulations details, different influences on the spectroelectrochemical responses in normal and parallel modes, experimental UV-vis spectrum of $AQ2S^-$.

ACKNOWLEDGEMENTS

The authors greatly appreciate the financial support provided by the Fundación Séneca de la Región de Murcia (Project 19887/GERM/15) and by the Ministerio de Ciencia e Innovación (PID2019-106097GB-I00/AEI/10.13039/501100011033), as well as for the very helpful advice on experimental design and measurements by Profs. A. Colina and A. Heras (University of Burgos, Spain).

REFERENCES

(1) Goor, G.; Glenneberg, J.; Jacobi, S.; Dadabhoy, J.; Candido, E. Hydrogen Peroxide. In *Ullmann's Encyclopedia of Industrial Chemistry*; John Wiley & Sons, Ltd: Weinheim, Germany, 2019; pp 1–40. https://doi.org/10.1002/14356007.A13_443.PUB3.

(2) Zhu, Q.; Pan, Z.; Hu, S.; Kim, J. H. Cathodic Hydrogen Peroxide Electrosynthesis Using Anthraquinone Modified Carbon Nitride on Gas Diffusion Electrode. *ACS Appl. Energy Mater.* **2019**, *2* (11), 7972–7979. https://doi.org/10.1021/acsaem.9b01445.

(3) Han, X. Bin; Ye, S. Structural Design of Oxygen Reduction Redox Mediators (ORRMs) Based on Anthraquinone (AQ) for the Li-O2Battery. *ACS Catal.* **2020**, *10* (17), 9790–9803. https://doi.org/10.1021/acscatal.0c01469.

(4) Matsuda, S.; Hashimoto, K.; Nakanishi, S. Efficient Li2O2 Formation via Aprotic Oxygen Reduction Reaction Mediated by Quinone Derivatives. *J. Phys. Chem. C* **2014**, *118* (32), 18397–18400. https://doi.org/10.1021/jp504894e.

(5) Hu, B.; Luo, J.; Hu, M.; Yuan, B.; Liu, T. L. A PH-Neutral, Metal-Free Aqueous Organic Redox Flow Battery Employing an Ammonium Anthraquinone Anolyte. *Angew. Chemie - Int. Ed.* **2019**, *131*, 16782–16789. https://doi.org/10.1002/anie.201907934.

(6) Ruan, W.; Mao, J.; Chen, Q. Redox Flow Batteries toward More Soluble Anthraquinone Derivatives. *Curr. Opin. Electrochem.* **2021**, *29*, 100748: 1-5. https://doi.org/10.1016/j.coelec.2021.100748.

(7) Malik, M. S.; Alsantali, R. I.; Jassas, R. S.; Alsimaree, A. A.; Syed, R.; Alsharif, M. A.; Kalpana, K.; Morad, M.; Althagafi, I. I.; Ahmed, S. A. Journey of Anthraquinones as Anticancer Agents-a Systematic Review of Recent Literature. *RSC Adv.* **2021**, *11* (57), 35806–35827. https://doi.org/10.1039/d1ra05686g.

(8) Omosa, L. K.; Midiwo, J. O.; Mbaveng, A. T.; Tankeo, S. B.; Seukep, J. A.; Voukeng, I. K.; Dzotam, J. K.; Isemeki, J.; Derese, S.; Omolle, R. A.; Efferth, T.; Kuete, V. Antibacterial Activities and Structure–Activity Relationships of a Panel of 48 Compounds from Kenyan Plants against Multidrug Resistant Phenotypes. *Springerplus* **2016**, *5* (1), 1–15. https://doi.org/10.1186/s40064-016-2599-1.

(9) Patel, O. P. S.; Beteck, R. M.; Legoabe, L. J. Antimalarial Application of Quinones: A Recent Update. *Eur. J. Med. Chem.* **2021**, *210*, 113084: 1-27. https://doi.org/10.1016/j.ejmech.2020.113084.

(10) Silva, T. L.; de Azevedo, M. de L. S. G.; Ferreira, F. R.; Santos, D. C.; Amatore, C.; Goulart, M. O. F. Quinone-Based Molecular Electrochemistry and Their Contributions to Medicinal Chemistry: A Look at the Present and Future. *Curr. Opin. Electrochem.* **2020**, *24*, 79–87. https://doi.org/10.1016/j.coelec.2020.06.011.

(11) Cervantes-González, J.; Vosburg, D. A.; Mora-Rodriguez, S. E.; Vázquez, M. A.; Zepeda, L. G.; Villegas Gómez, C.; Lagunas-Rivera, S. Anthraquinones: Versatile Organic Photocatalysts. *ChemCatChem* **2020**, *12* (15), 3811–3827. https://doi.org/10.1002/cctc.202000376.

(12) Liu, N.; Sun, G. Production of Reactive Oxygen Species by Photoactive Anthraquinone Compounds and Their Applications in Wastewater Treatment. *Ind. Eng. Chem. Res.* **2011**, *50* (9), 5326–5333. https://doi.org/10.1021/ie101423v.

(13) DeLiberto, S. T.; Werner, S. J. Review of Anthraquinone Applications for Pest Management and Agricultural Crop Protection. *Pest Manag. Sci.* **2016**, *72* (10), 1813–1825. https://doi.org/10.1002/ps.4330.

(14) O'Brien, P. J. Molecular Mechanisms of Quinone Cytotoxicity. *Chem. Biol. Interact.* **1991**, *80* (1), 1–41. https://doi.org/10.1016/0009-2797(91)90029-7.

(15) Quan, M.; Sanchez, D.; Wasylkiw, M. F.; Smith*, D. K. Voltammetry of Quinones in Unbuffered Aqueous Solution. *J Am Chem Soc* **2007**, *129* (8), 12847–12856. https://doi.org/10.1021/ja0743083.

(16) Li, Q.; Batchelor-McAuley, C.; Lawrence, N. S.; Hartshorne, R. S.; Compton, R. G. Electrolyte Tuning of Electrode Potentials: The One Electron vs. Two Electron Reduction of Anthraquinone-2-Sulfonate in Aqueous Media. *Chem. Commun.* **2011**, *47* (41), 11426–11428. https://doi.org/10.1039/c1cc14191k.

(17) Laborda, E.; Gómez-Gil, J. M.; Molina, A. Microelectrode Voltammetry of Multi-Electron Transfers Complicated by Coupled Chemical Equilibria: A General Theory for the Extended Square Scheme. *Phys. Chem. Chem. Phys.* **2017**, *19* (25), 16464–16476. https://doi.org/10.1039/C7CP02135F.

(18) Evans, D. H. One-Electron and Two-Electron Transfers in Electrochemistry and Homogeneous Solution Reactions. *Chem. Rev.* **2008**, *108* (7), 2113–2144.

(19) Hammerich, O.; Speiser, B. *Organic Electrochemistry*; CRC Press: Boca Raton, 2016.

(20) Barrière, F.; Geiger, W. E. Use of Weakly Coordinating Anions to Develop an Integrated

Approach to the Tuning of ΔE1/2 Values by Medium Effects. *J. Am. Chem. Soc.* **2006**, *128* (12), 3980–3989. https://doi.org/10.1021/ja058171x.

(21) Savéant, J.; Costentin, C. *Elements of Molecular and Biomolecular Electrochemistry*; John Wiley & Sons: Hoboken, NJ, 2019. https://doi.org/10.1002/9781119292364.

(22) Bard, A. J.; Faulkner, L. R. *Electrochemical Methods: Fundamentals and Applications*, 2nd ed.; Wiley: New York, 2001.

(23) Molina, A.; González, J. *Pulse Voltammetry in Physical Electrochemistry and Electroanalysis*; Scholz, F., Ed.; Monographs in Electrochemistry; Springer International Publishing: Berlin, 2016. https://doi.org/10.1007/978-3-319-21251-7.

(24) Compton, R. G.; Banks, C. E. *Understanding Voltammetry*, 3rd ed.; World Scientific, 2018. https://doi.org/10.1142/q0155.

(25) Evans, D. H.; Hu, K. Inverted Potentials in Two-Electron Processes in Organic Electrochemistry. *J. Chem. Soc. - Faraday Trans.* **1996**, *92* (20), 3983–3990. https://doi.org/10.1039/ft9969203983.

(26) Andrieux, C. P.; Savéant, J. M. Electro-Oxidation of 1,2-Ene-Diamines. *J. Electroanal. Chem.* **1970**, *28* (2), 339–348. https://doi.org/10.1016/S0022-0728(70)80128-0.

(27) Belding, S. R.; Baron, R.; Dickinson, E. J. F.; Compton, R. G. Modeling Diffusion Effects for a Stepwise Two-Electron Reduction Process at a Microelectrode: Study of the Reduction of Para-Quaterphenyl in Tetrahydrofuran and Inference of Fast Comproportionation of the Dianion with the Neutral Parent Molecule. *J. Phys. Chem. C* **2009**, *113* (36), 16042–16050. https://doi.org/10.1021/jp906323n.

(28) Lehmann, M. W.; Evans, D. H. Effect of Comproportionation on Voltammograms for Two-Electron Reactions with an Irreversible Second Electron Transfer. *Anal. Chem.* **1999**, *71* (10), 1947–1950. https://doi.org/10.1021/ac990066g.

(29) Belding, S. R.; Limon-Petersen, J. G.; Dickinson, E. J. F.; Compton, R. G. Cyclic Voltammetry in the Absence of Excess Supporting Electrolyte Offers Extra Kinetic and Mechanistic Insights: Comproportionation of Anthraquinone and the Anthraquinone Dianion in Acetonitrile. *Angew. Chemie - Int. Ed.* **2010**, *122*, 9428 –9431. https://doi.org/10.1002/anie.201004874.

(30) Boisseau, R.; Bussy, U.; Giraudeau, P.; Boujtita, M. In Situ Ultrafast 2D NMR Spectroelectrochemistry for Real-Time Monitoring of Redox Reactions. *Anal. Chem.*

2015, *87* (1), 372–375. https://doi.org/10.1021/ac5041956.

(31) Danis, A. S.; Potts, K. P.; Perry, S. C.; Mauzeroll, J. Combined Spectroelectrochemical and Simulated Insights into the Electrogenerated Chemiluminescence Coreactant Mechanism. *Anal. Chem.* **2018**, *90* (12), 7377–7382. https://doi.org/10.1021/acs.analchem.8b00773.

(32) Holubowitch, N. E.; Crabtree, C.; Budimir, Z. Electroanalysis and Spectroelectrochemistry of Nonaromatic Explosives in Acetonitrile Containing Dissolved Oxygen. *Anal. Chem.* **2020**, *92* (17), 11617–11626. https://doi.org/10.1021/acs.analchem.0c01174.

(33) Amatore, C.; Klymenko, O.; Svir, I. A New Strategy for Simulation of Electrochemical Mechanisms Involving Acute Reaction Fronts in Solution: Application to Model Mechanisms. *Electrochem. commun.* **2010**, *12* (9), 1165–1169. https://doi.org/10.1016/j.elecom.2010.06.008.

(34) Zhao, E. W.; Jónsson, E.; Jethwa, R. B.; Hey, D.; Lyu, D.; Brookfield, A.; Klusener, P. A. A.; Collison, D.; Grey, C. P. Coupled in Situ NMR and EPR Studies Reveal the Electron Transfer Rate and Electrolyte Decomposition in Redox Flow Batteries. *J. Am. Chem. Soc.* **2021**, *143* (4), 1885–1895. https://doi.org/10.1021/jacs.0c10650.

(35) Martín-Yerga, D.; Pérez-Junquera, A.; González-García, M. B.; Perales-Rondon, J. V.; Heras, A.; Colina, A.; Hernández-Santos, D.; Fanjul-Bolado, P. Quantitative Raman Spectroelectrochemistry Using Silver Screen-Printed Electrodes. *Electrochim. Acta* **2018**, *264*, 183–190. https://doi.org/10.1016/j.electacta.2018.01.060.

(36) Takao, K.; Tsubomura, T. Design and Demonstration of Absorption/Luminescence-Compatible Spectroelectrochemical Cell with Optically Transparent Thin-Layer Electrode. *J. Electroanal. Chem.* **2022**, *911*, 116217: 1-6. https://doi.org/10.1016/j.jelechem.2022.116217.

(37) Appleby, C. A.; Morton, R. K. Lactic Dehydrogenase and Cytochrome B2 of Baker's Yeast; Purification and Crystallization. *Biochem. J.* **1959**, *71* (3), 492–499. https://doi.org/10.1042/bj0710492.

(38) Gamage, R. S. K. A.; McQuillan, A. J.; Peake, B. M. Ultraviolet-Visible and Electron Paramagnetic Resonance Spectroelectrochemical Studies of the Reduction Products of Some Anthraquinone Sulphonates in Aqueous Solutions. *J. Chem. Soc. Faraday Trans.*

1991, *87* (22), 3653–3660. https://doi.org/10.1039/FT9918703653.

FOR TABLE OF CONTENTS ONLY